Physica Medica 72 (2020) 32–38

Contents lists available at ScienceDirect

Physica Medica

journal homepage: www.elsevier.com/locate/ejmp

Original paper

Quantitative evaluation of transmission properties of breast tissue equivalent materials under Compton scatter imaging setup

Kai Yang[a,*,1], Changran Geng[b,1], Xinhua Li[a], Bob Liu[a]

[a] Division of Diagnostic Imaging Physics, Department of Radiology, Massachusetts General Hospital, 55 Fruit Street, Boston, MA 02114, United States
[b] Department of Nuclear Science and Technology, Nanjing University of Aeronautics and Astronautics, Nanjing 211106, People's Republic of China

ARTICLE INFO

Keywords:
Compton scattering
Breast imaging
Transmission
Monte Carlo simulation

ABSTRACT

To explore the potential of utilizing Compton scattered x-ray photons for imaging applications, it is critical to accurately evaluate scattered x-ray transmission properties of targeted tissue materials. In this study, scattered x-ray transmission of breast tissue equivalent phantoms was evaluated. Firstly, two validations were carried out using a primary x-ray beam at 80 kVp with both experimental measurement (ion chamber with narrow-beam setup) and analytical calculation (Spektr toolkit). The tungsten-anode x-ray spectrum model was thus validated by measuring and calculating the transmission through increasing thickness of 1100 Aluminum filters. Similarly, the composition models of breast tissue equivalent phantoms (CIRS, 012A) were validated by measuring and calculating x-ray transmission for three different breast compositions (BR30/70, BR50/50, and BR70/30). Following validation, transmission properties of Compton scattered x-ray photons were measured with a GOS based linear array detector at the 90° angle from the primary beam. The same study was performed through three independent approaches: experimental measurement, analytical calculation, and Monte Carlo simulation (GEANT4). For all three methods, the scattered x-ray photon transmission as functions of phantom thickness were determined and fit into exponential functions. The transmission curves from all three methods matched reasonably well, with a maximum difference of 6.3% for the estimated effective attenuation coefficients of the BR50/50 phantom. The relative difference among the three methods of estimated attenuation is under 3.5%. As an initial step to develop a novel Compton scatter-based breast imaging system, the quantitative results from this study paved a fundamental base for future work.

1. Introduction

In the photon energy range used for diagnostic x-ray exams (~20–140 keV), Compton scattering is the dominant interaction between x-ray photons and human soft tissue. However, the x-ray detection and image formation are all based on the "straight-line" assumption and only the total linear attenuation through the imaging target is utilized as the source of image contrast. For the current scheme of clinical x-ray imaging, the scattered photons were either undetected (scattered off the source-to-detector pathway, causing radiation safety concerns), rejected (by anti-scatter grid), or incorrectly detected with primary photons without differentiation. It is challenging to solely use Compton scattered photons for imaging purpose. Only shallow information can be provided with backscatter setup and limited success had been demonstrated in the archaeology field and industrial non-destructive examination [1–4]. To detect Compton scattered photons generated within greater depth of the object (with certain approach to reject photons from multiple scatter), many previously proposed methods [5–9] had to rely on monoenergetic x-ray sources and still had major challenges to determine two key factors: the location of the Compton interaction and the attenuation of the Compton scattered photons before detection. Both information relies on the imaging object itself. So, there's no theoretical viable solution. Most studies either assumed uniform water-equivalent background, or only applied to small sized specimen samples [10–12] (Fig. 1-a and b). Either method won't provide satisfying solutions or practical "image" of the object.

Hypothetically speaking, if Compton scattered photons can be directly detected from an existing x-ray projection system (Fig. 1-c), it will bring two key advantages: 1. the added secondary image contrast mechanism to the existing primary contrast for x-ray imaging; 2. the reduced radiation shielding requirement for the system with added detectors as secondary barriers. Several other different approaches had

* Corresponding author.
E-mail address: kyang11@mgh.harvard.edu (K. Yang).
[1] These authors contributed equally to this work.

https://doi.org/10.1016/j.ejmp.2020.03.014
Received 25 October 2019; Received in revised form 12 February 2020; Accepted 10 March 2020

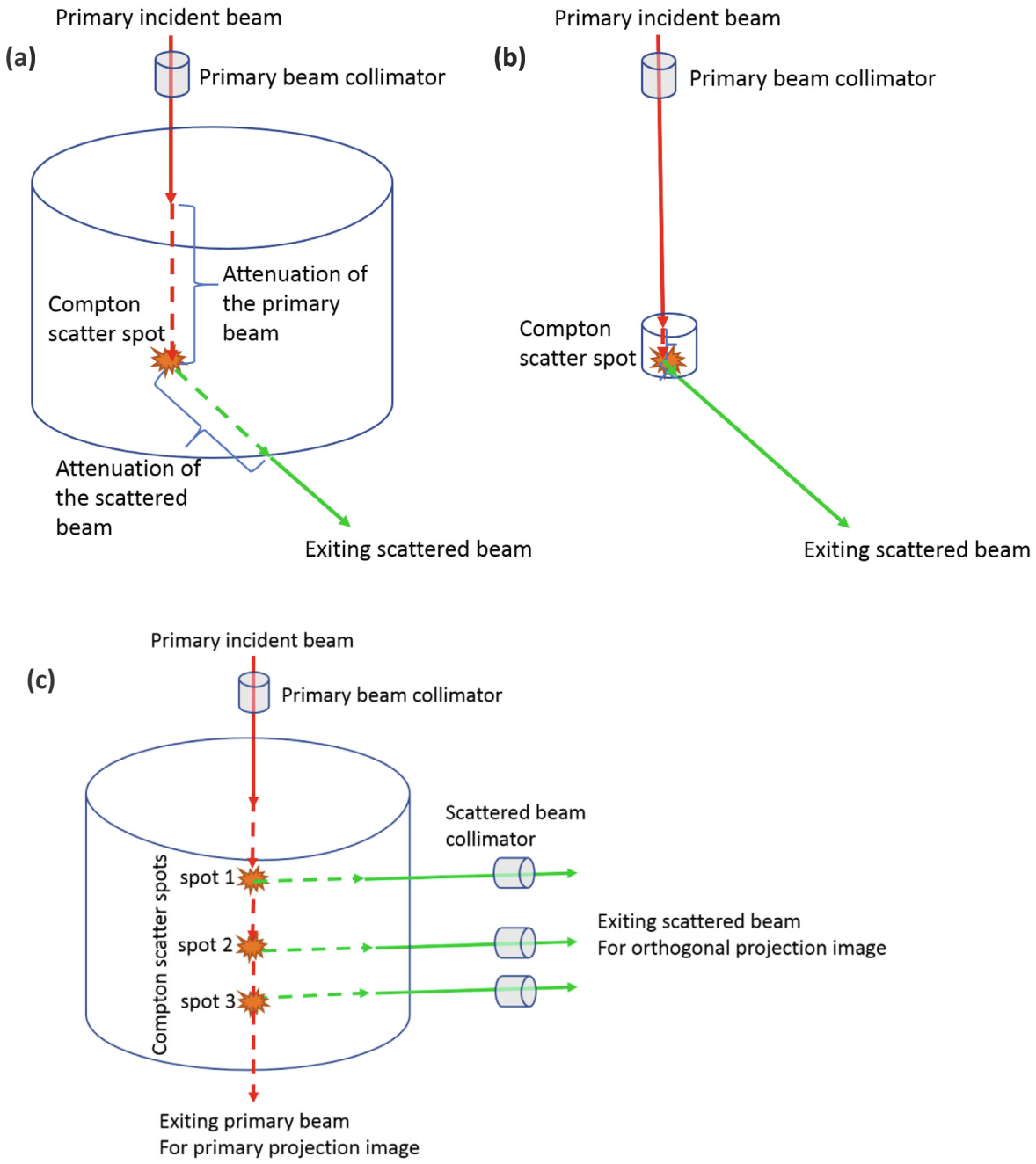

Fig. 1. Conceptual diagram for different approaches utilizing Compton scatter. (a): Traditional way with large object, the attenuation paths (brackets) are undetermined. (b): Traditional way for small-sized specimen object, which cannot be utilized for in vivo imaging. (c): Our approach presented in this study, which will provide "additional" information from the primary projection image.

been proposed with preliminary setups [13–16]. As a preliminary study to explore the feasibility to utilize scattered x-ray photons for imaging, this study focuses on the application of breast imaging when scattered photons are detected at the 90-degree angle. We would like to emphasize that in this approach we do not make any assumptions on the imaging object, nor do we try to decipher the Compton scatter coefficients of the interaction spot. On the other hand, we will generate projection images which provide additional depth information other than just the primary beam projection radiograph. Like all x-ray related imaging system development, the first step is to accurately evaluate x-ray transmission properties of scattered x-ray photons through targeted tissue materials. Therefore, the purpose of this study was to use the Compton scattered photons from tissue equivalent phantoms as the additional x-ray source and then evaluate the transmission profiles through different tissue equivalent materials. We performed the study using three different approaches with experimental measurement, analytical calculation, and Monte Carlo simulation.

2. Methods and materials

2.1. X-ray spectrum model and phantom composition model validation

The experimental measurements in this study were all performed from a clinical radiographic system (DX-D600, AGFA, Morse, Belgium).

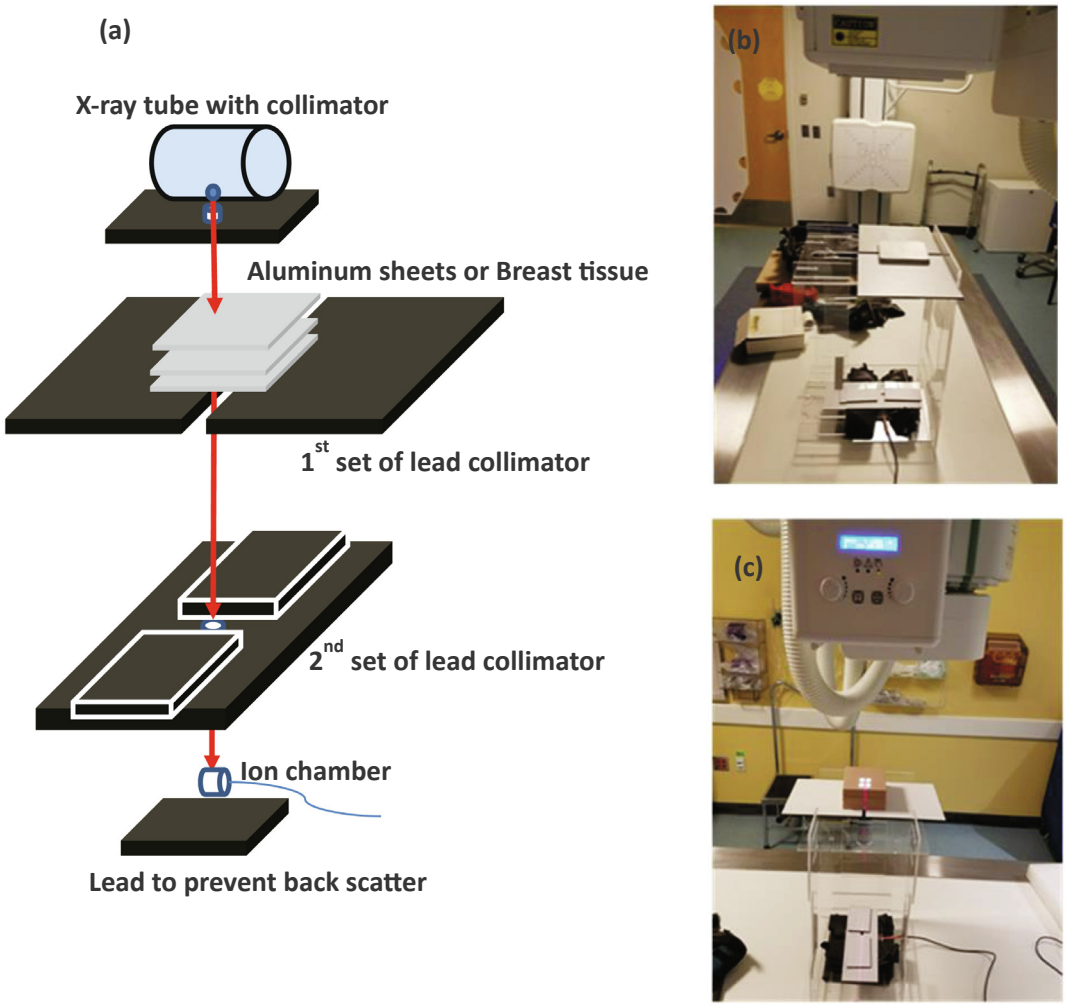

Fig. 2. Narrow-beam transmission measurements with an ion chamber. Two sets of lead sheets were added to reject scatter. (a): Diagram for the setup (for illustration purpose, distance not to scale). (b): Transmission measurements through aluminum for spectral validation. (c): Transmission measurements through breast tissue equivalent material for material composition model validation.

To provide input data for analytical calculation and Monte Carlo simulation, the x-ray spectrum model and the phantom material were first validated. As shown in Fig. 2, the x-ray spectrum model using TASMIP [17] via Spektr [18] (in MATLAB, Natick MA) was validated by measuring and calculating the transmission through increasing thickness of 1100 Aluminum filters (10 cm × 10 cm) with a 0.6 cc thimble ionization chamber (10x6-0.6CT, Radcal, Morovia, CA). The ion chamber had an effective length of 19.7 mm and was calibrated by the manufacturer with equipment traceable to NIST standard for the HVL range of 3–20 mm Al.

Several key details were implemented to best set up a narrow-beam geometry. The x-ray field was tightly collimated (4 mm × 9 mm at 100 cm from focal spot) by manual adjustment of the collimator. The ion chamber and the aluminum sheets were placed at 128 cm and 64 cm away from the focal spot, respectively. In addition, two sets of lead sheets were added to minimize scatter, with one set just below the aluminum sheets and one set just above the ion chamber. The parameters used for measurements were 80 kVp (with HVL of 3.2 mm Al), 50 mAs. The aluminum sheet thickness was incremental from 0.5 to 9 mm (specifically 0.5, 1, 2, 3, 4, 5, 7, and 9 mm). With the measured transmission data, the inherent tube filtration was iteratively determined using Spektr with the TASMIP model.

The next step was to validate the elemental composition models of breast tissue equivalent phantoms used this study. From the CIRS 012A phantom series (CIRS, Norfolk, VA), three uniform sets were tested for different glandular/adipose percentages (BR30/70, BR50/50, and BR70/30). With the exactly same narrow-beam setup as the spectrum validation (Fig. 2), phantom blocks with increasing thickness (0.5, 1, 2, 3, 5, 7 cm) were placed in the x-ray beam and the transmission was determined through the measurements by the ion chamber. Using the spectral model confirmed above and the manufacturer provided elemental composition information, the transmission data were calculated analytically using Spektr and compared to the experimentally measured data.

The calculation details for the above two steps are straightforward and not included in this study for brevity. Very similar examples can be referred to a previous study [19].

2.2. Transmission measurements with Compton scattered photons

As shown in Fig. 3, with the same x-ray system, minimally-collimated (2 mm × 3 mm at 100 cm from focal spot) primary x-ray beam was targeted onto a tissue equivalent block (BR50/50, CIRS 012A). The scattered photons were detected at a 90-degree angle to the incident primary beam, using a solid-state linear array detector, which is a GOS scintillator based indirect detector (X-Scan 0.8f3-512, Detection Technology Inc, Finland). This detector (referred to as “DT detector” below) is composed of a linear array of 640 pixels with pixel dimension of

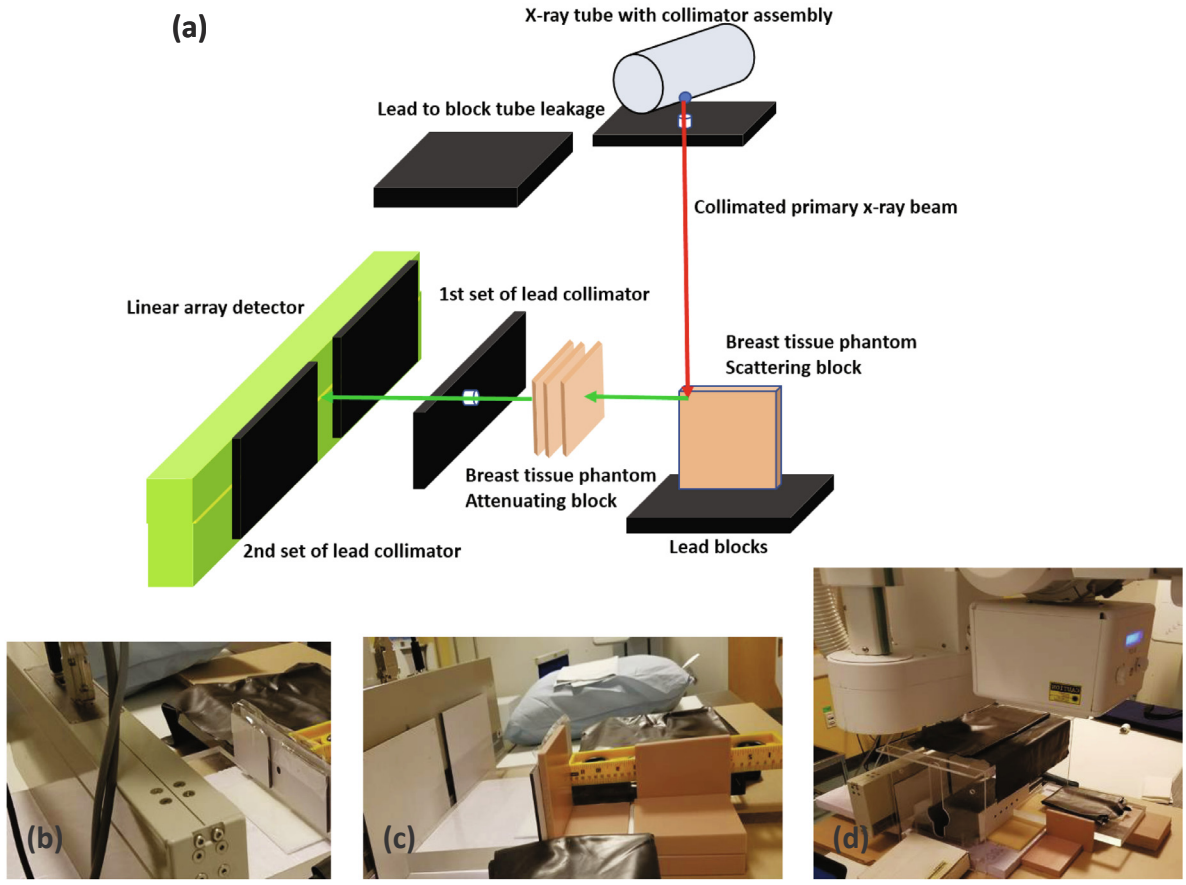

Fig. 3. Experiment setup for Compton scatter measurements. (a): Overview diagram of the setup (for illustration purpose, distance not to scale). The arrows indicate the primary and scattered x-ray photon path. Two different sets of lead collimators were used to reject x-ray signals not going along the path defined by the green arrow. (b)–(d): Pictures of the setup, including (b) the detector and 1st set of lead collimator, (c) the breast tissue phantom and 2nd set of lead collimator, and (d) lead sheets to block tube leakage and scatter from tube assembly. The lead thickness was all 2 mm and above.

0.8 mm × 0.7 mm. This detector had been previously utilized to measure scatter signal from a Digital Breast Tomosynthesis system for shielding purpose [20,21] and had demonstrated high detection sensitivity, which was crucial for this experiment. The x-ray focal spot is 65 cm away from the top of the scattering block. The 1st set of lead collimator (back end of the scattering block) is 10 cm away from the attenuating block and 20 cm away from the DT detector. To achieve the best data quality under the geometry of "pencil-beam-in and pencil-beam-out", double lead collimators with very small openings (as shown as the 1st plus 2nd set of collimators) were added right behind the phantom and in front of the detector. It is worth noting that additional lead shielding was also added to minimize x-ray tube leakage and scattering from the tube assembly and the experiment table.

The parameters used for measurements were 80 kVp, 500 ms, 320 mAs. The detector integration time was set as 10 ms and therefore 50 readings per exposure. With the narrow collimation setup (Fig. 3), twelve detector pixels were used to detect the scattered photons. The standard deviations between the 12 × 50 = 600 measurements was used to estimate the measurement uncertainty. The averaged signal from these 600 measurements was used to reduce noise. Two groups of transmission data were measured: same material (BR50/50) with different thickness (0.5–5 cm) and same thickness (1 cm) with different materials (BR30/70, BR50/50, BR70/30).

2.3. Analytical calculation of transmission of Compton scattered photons

With the x-ray spectrum and phantom materials confirmed in Section 2.1. A, a simple analytical calculation model was set up using the Spektr toolkit to evaluate transmission properties of Compton scattered photons through different phantom materials.

Assuming the primary incident x-ray spectrum is $\Phi_0(kV, E)$, which is photon fluence with units of photons/mm^2 and the linear Compton scatter coefficient of the BR50/50 material is $\sigma(E)$ (in cm^{-1}). After the initial interaction at the top 1 mm layer of the scattering block, the new spectrum at the 90-degree scattering angle is determined as:

$$\Phi_{c90}(kVp, E') = \Phi_0(kV, E)(1 - e^{-0.1\cdot\sigma(E)}) \quad (1)$$

where $E' = \frac{E}{1+\frac{E}{511keV}}$, and $E \in [0, kVp]$.

The scattered signal detected by the DT detector after the attenuation through x cm of phantom material is:

$$I(kVp, x) = \int_0^{kVp} \Phi_{c90}(kV, E')e^{-x\cdot\mu(E')}D(E')dE' \quad (2)$$

where $I(kVp, x)$ is unit-less digit number output from the detector, $\mu(E')$ is the linear attenuation coefficient for the attenuating material in cm^{-1}. $D(E)$ is the response of the DT detector as modeled previously for a 0.1 mm Aluminum window plus a 0.8 mm GOS block [19] as:

$$D(E) = k_{GOS}e^{-\mu_{Al}(E)\cdot 0.01}E\left(1 - e^{-\mu_{GOS}(E)\cdot 0.08}\right) \quad (3)$$

The transmission was then calculated as:

$$\Gamma(kVp, x) = \frac{I(kVp, x)}{I(kVp, 0)} \quad (4)$$

Therefore k_{GOS}, the scaling constant in Eq. (3) was cancelled out.

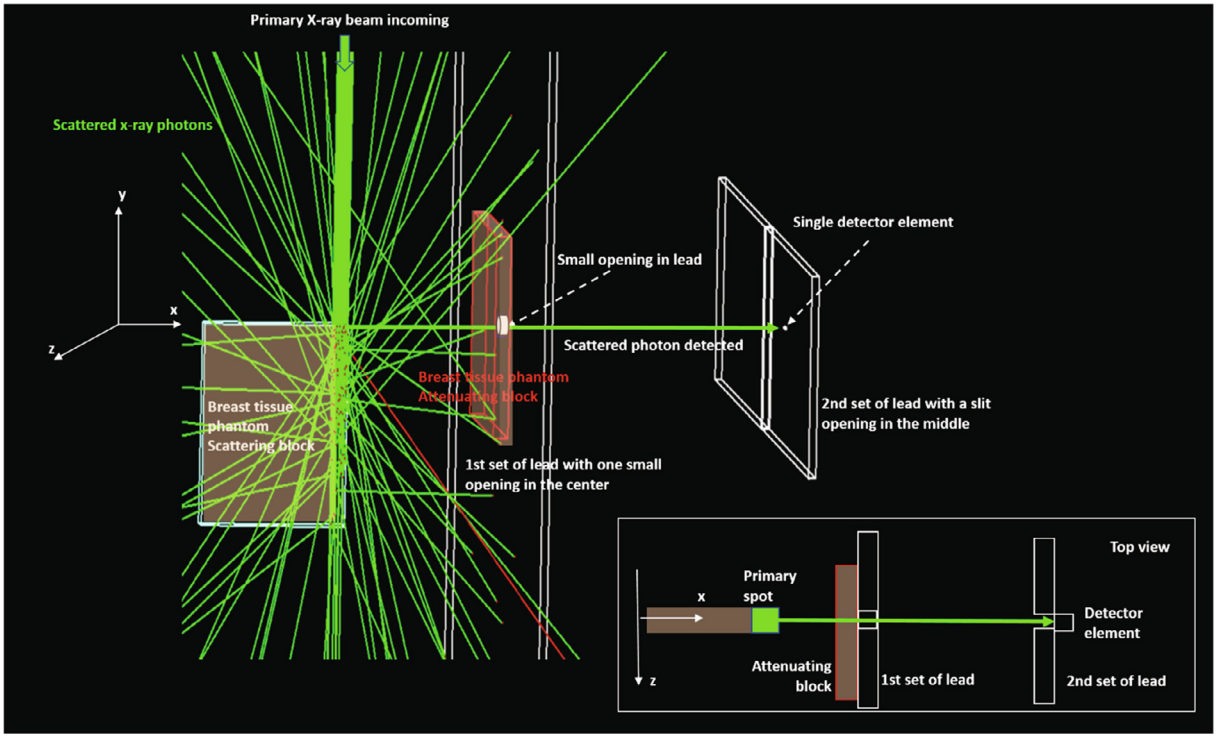

Fig. 4. Monte Carlo simulation model. The setup was to closely match the experiment setup shown in Fig. 3. Primary x-ray beam travels down along the y-axis with the scattering tissue block placed within the x-y plane at z = 0. Two sets of lead collimators (1st and 2nd to match Fig. 3) with a thickness of 5 mm were placed parallel to the y-z plane and at x = 10 cm and 30 cm, respectively. The attenuating block with various material and thickness was placed right in front of the 1st set of lead. The green lines shown are x-ray photon tracks and the red lines are electron tracks.

2.4. Monte Carlo simulation

The Monte Carlo simulation was performed by the Geant4 toolkit (Geant4.10.2), which was well validated for photon and charged particle simulation [22]. The Penelope electromagnetic physics list (with energy range down to a few hundred eV) was used to cover the relatively low energy range (keV) of this study. A 1 × 1 cm^2 square beam was used as the incident primary beam. In line with the above experiment setup, we set up the Monte Carlo simulation model as shown in Fig. 4. For simplification, only a single individual GOS detector element (0.7 mm × 0.8 mm) was simulated. The incident energy was sampled according to the spectrum from the result of Section 2.1. A. For each simulation, 1×10^8 histories were tracked on a Linux cluster platform (Partners ERISone). A total of 1000 simulations for each attenuating block material (BR3070, BR5050, BR7030) and thickness (0, 1, 2, 3, 4, and 5 cm) were performed.

3. Results

3.1. X-ray spectrum model and phantom materials validation

Fig. 5 shows the transmission profiles for increasing thickness for Al sheets (Fig. 5-a) and breast tissue equivalent blocks (Fig. 5-b). The results from experimental measurements and analytical calculations had very good agreements. Therfore the spectrum model and the phantom materials were validated for the analytical calculation and Monte Carlo simulation for tranmission evaluation of the Compton scattered photons.

3.2. Compton scattered photon transmission

Fig. 6 shows the comparison of photon transmission profiles through increasing thickness of BR50/50 blocks. Data from three methods (Monte Carlo simulation, experimental measurements, analytical calculation) all agreed to each other very well. The transmission decreases as the phantom thickness increasing, closely following an exponential curve (as shown by the trend lines). The transmission data was fitted to the phantom thickness with a single term exponential function as $\Gamma(x) = ae^{-bx}$. Approximately considered as the "effective attenuation coefficient" of the given material and thickness, the fitting parameter "b" in the unit of mm^{-1}, was 0.0254, 0.0238, and 0.0251, for Monte Carlo, experimental measurements, and analytical calculation, respectively. The largest difference is 6.3% between all three methods. Again, given the polyenergetic nature of x-ray spectrum (and the Compton scattered x-ray spectrum), a single exponential curve as the simple Beer-Lambert law in theory cannot fully describe the transmission profiles. Therefore, the fitting parameters shown above can only be used as a rough approximation of the overall attenuation of the material.

Table 1 summerizes the tranmisson comparison for three different materials with the same thickness of 1 cm. The maximal difference between all three methods is 3.5%. For Monte Carlo method, the mean and standard deviation of the attenuation coefficients were estimated from the results of the 1000 simulation runs.

The differences in transmission between different phantom material is relatively small, given the subtle differences in the adipose/glandular percentage.

4. Discussion

At the very initial stage of developing a new Compton scatter imaging system, many practical questions remain unanswered, including the optimal system geometry and the primary x-ray spectrum, which directly affects the trade-off between the contrast-to-noise ratio (CNR) of the image and the radiation dose to the object. In this study, only 80 kVp was tested, based on previous experience from dedicated breast CT [23,24]. However, the data clearly showed the promising nature of utilizing scattered photons given that the transmission

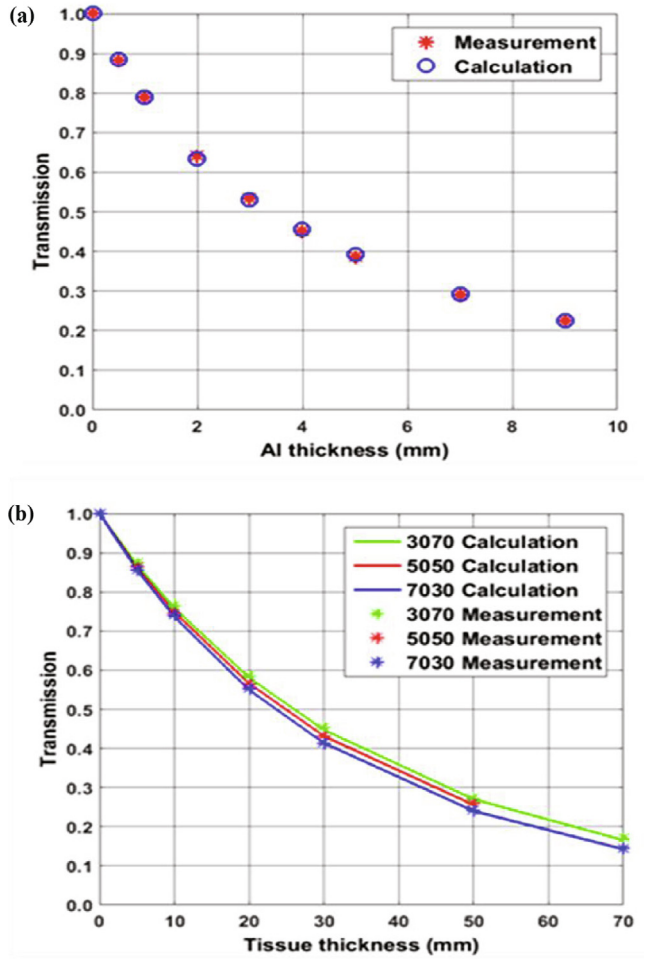

Fig. 5. Transmission profile results. (a) Transmission through incremental Al sheets. (b) Transmission through incremental breast tissue equivalent blocks.

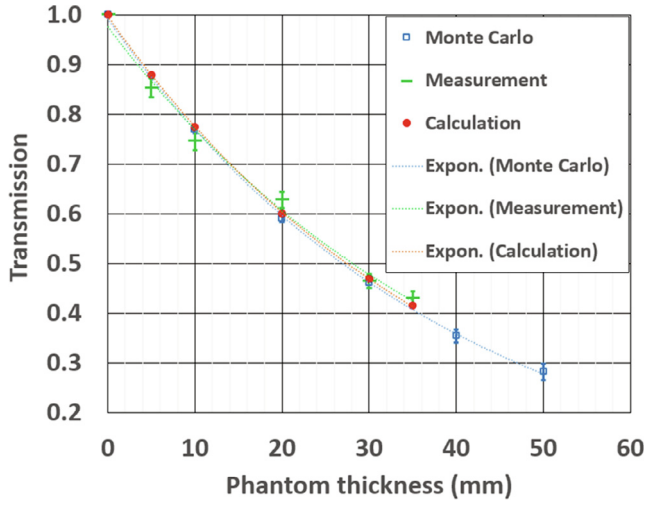

Fig. 6. Transmission profile results for BR50/50. Error bars were provided for Monte Carlo simulation and experimental measurements. Exponential fittings were applied to all three groups of data.

properties can be accurately measured and calculated. The current setup is assuming a pencil beam primary incidence and a pencil beam scatter detection. The main reason is to help the localization of the scatter interaction and reject x-rays which underwent multiple scatters. Apparently, this "*pencil-beam-in and pencil-beam-out*" setup requires the modification of the existing primary imaging system and has a relatively low detection efficiency of scattered photons. This geometry might be further optimized to improve the detection efficiency, together with other system parameter optimizations through a more comprehensive study.

Table 1
Transmission data through 1 cm phantom material.

Phantom	Monte Carlo	Std	Measurement	std	Calculation	Max % Diff.
BR3070	0.7716	0.0069	0.7574	0.0172	0.7820	3.1%
BR5050	0.7694	0.0067	0.7464	0.0182	0.7737	3.5%
BR7030	0.7372	0.0065	0.7463	0.0168	0.7641	3.5%

5. Conclusions

It is the first time to quantitatively evaluate the transmission/attenuation properties of breast tissue equivalent materials under Compton scatter imaging setup. The initial results from this study demonstrated the potential characteristics of Compton scatter imaging for breast imaging applications. Even though we focused our study on breast imaging, results in this study can also be applied to other potential applications, including general radiography and imaging guidance for radiation oncology treatment.

Declaration of Competing Interest

The authors declare that they have no known competing financial interests or personal relationships that could have appeared to influence the work reported in this paper.

Acknowledgments

This work used the High-Performance Clusters of the Partners Cooperation for Monte Carlo simulation, and the authors thank the Enterprise Research at Partners Healthcare for their in-depth support.

References

[1] Tondon A, Singh M, Sandhu BS, Singh B. Non-destructive study of wood using the Compton scattering technique. Appl Radiat Isot 2017;129:204–10.
[2] Harding G, Kosanetzky J. Scattered X-ray beam nondestructive testing. Nucl Instrum Methods Phys Res Sect A 1989;280(2–3):517–28.
[3] Harding G, Harding E. Compton scatter imaging: a tool for historical exploration. Appl Radiat Isot 2010;68(6):993–1005.
[4] Harding G. Inelastic photon scattering: effects and applications in biomedical science and industry. Radiat Phys Chem 1997;50(1):91–111.
[5] Norton Stephen J. Compton scattering tomography. J Appl Phys 1994;76(4):2007–15.
[6] Battista JJ, Bronskill MJ. Compton scatter imaging of transverse sections: an overall appraisal and evaluation for radiotherapy planning. Phys Med Biol 1981;26(1):81–99.
[7] Battista JJ, Bronskill MJ. Compton-scatter tissue densitometry: calculation of single and multiple scatter photon fluences. Phys Med Biol 1978;23(1):1–23.
[8] Antoniassi M, Conceicao AL, Poletti ME. Study of electron densities of normal and neoplastic human breast tissues by Compton scattering using synchrotron radiation. Appl Radiat Isot 2012;70(7):1351–4.
[9] Antoniassi M, Conceicao AL, Poletti ME. Compton scattering spectrum as a source of information of normal and neoplastic breast tissues' composition. Appl Radiat Isot 2012;70(7):1451–5.
[10] Ryan EA, Farquharson MJ. Breast tissue classification using x-ray scattering measurements and multivariate data analysis. Phys Med Biol 2007;52(22):6679–96.
[11] Ryan EA, Farquharson MJ, Flinton DM. The use of Compton scattering to differentiate between classifications of normal and diseased breast tissue. Phys Med Biol 2005;50(14):3337–48.
[12] Shimao D, Sunaguchi N, Sasaya T, Yuasa T, Ichihara S, Kawasaki T, et al. Imaging with ultra-small-angle X-ray scattering using a Laue-case analyzer and its application to human breast tumors. Phys Med 2017;44:236–42.
[13] Van Uytven E, Pistorius S, Gordon R. A method for 3D electron density imaging using single scattered x-rays with application to mammographic screening. Phys Med Biol 2008;53(19):5445–59.
[14] Van Uytven E, Pistorius S, Gordon R. An iterative three-dimensional electron

density imaging algorithm using uncollimated compton scattered x rays from a polyenergetic primary pencil beam. Med Phys 2007;34(1):256–65.
[15] Yan H, Tian Z, Shao Y, Jiang SB, Jia X. A new scheme for real-time high-contrast imaging in lung cancer radiotherapy: a proof-of-concept study. Phys Med Biol 2016;61(6):2372–88.
[16] Prettyman TH, Gardner RP, Russ JC, Verghese K. A combined transmission and scattering tomographic approach to composition and density imaging. Appl Radiat Isot 1993;44(10–11):1327–41.
[17] Boone JM, Seibert JA. An accurate method for computer-generating tungsten anode x-ray spectra from 30 to 140 kV. Med Phys 1997;24(11):1661–70.
[18] Siewerdsen JH, Waese AM, Moseley DJ, Richard S, Jaffray DA. Spektr: a computational tool for x-ray spectral analysis and imaging system optimization. Med Phys 2004;31(11):3057–67.
[19] Yang K, Li X, George Xu X, Liu B. Direct and fast measurement of CT beam filter profiles with simultaneous geometrical calibration. Med Phys 2017;44(1):57–70.
[20] Yang K, Li X, Liu B. Scatter radiation intensities around a clinical digital breast tomosynthesis unit and the impact on radiation shielding considerations. Med Phys 2016;43(3):1096–110.
[21] Yang K, Schultz TJ, Li X, Liu B. Radiation shielding calculation for digital breast tomosynthesis rooms with an updated workload survey. J Radiol Prot 2017;37(1):230–46.
[22] Sea Agostinelli, John Allison, K al Amako, J Apostolakis, H Araujo, P Arce, M Asai, D Axen, S Banerjee, and G Barrand, “GEANT4—a simulation toolkit,” Nuclear instruments and methods in physics research section A: Accelerators, Spectrometers, Detectors and Associated Equipment 506 (3), 250-303 (2003).
[23] John M Boone, Thomas R Nelson, Karen K Lindfors, and J Anthony Seibert, “Dedicated breast CT: radiation dose and image quality evaluation,” Radiology 221 (3), 657-667 (2001).
[24] Karen K Lindfors, John M Boone, Thomas R Nelson, Kai Yang, Alexander LC Kwan, and DeWitt F Miller, “Dedicated breast CT: initial clinical experience,” Radiology 246 (3), 725-733 (2008).